Journal of Alloys and Compounds 764 (2018) 267–278

Contents lists available at ScienceDirect

Journal of Alloys and Compounds

journal homepage: http://www.elsevier.com/locate/jalcom

The correlation of microstructure features, dry sliding wear behavior, hardness and tensile properties of Al-2wt%Mg-Zn alloys

Bernardo P. Reis [a], Maiquel M. Lopes [a], Amauri Garcia [b], Carlos A. dos Santos [a, *]

[a] Pontifícia Universidade Católica do Rio Grande do Sul – PUCRS, School of Technology, Av. Ipiranga, 6681, 90.619-900, Porto Alegre, RS, Brazil
[b] Universidade de Campinas - UNICAMP, Department of Manufacturing and Materials Engineering, 13083-860, Campinas, SP, Brazil

ARTICLE INFO

Article history:
Received 22 March 2018
Received in revised form
6 June 2018
Accepted 7 June 2018
Available online 15 June 2018

Keywords:
Al-Mg-Zn alloys
Solidification
Microstructures
Mechanical properties
Wear

ABSTRACT

The effect of Zn addition on the as-cast microstructures, mechanical properties and dry sliding wear behavior of Al-2wt%Mg-Zn alloys is investigated in this study. Two Al-Zn-Mg ternary alloys, with 5% and 8% Zn contents and 2 wt% Mg, were developed: 752 alloy (Al-5wt%Zn - 2 wt%Mg) and 782 alloy (Al-8wt% Zn-2wt%Mg). Unidirectional vertical upward solidification experiments were performed using a metallic water-cooled mold instrumented by thermocouples. Samples extracted along the length of the resultant ingots were characterized by optical microscopy (OM), scanning electron microscopy (SEM), energy dispersive spectroscopy (EDS), and X-ray diffraction (XRD), and mechanical properties were analyzed by hardness, microhardness, tensile and dry sliding wear tests. The results showed that the microstructures for both alloys are composed of an α-Al dendritic matrix and $MgZn_2$ and $Al_2Mg_3Zn_3$ interdendritic precipitates. An experimental equation is derived relating the secondary dendrite arm spacing (λ_2) to the solidification cooling rate ($\dot{T}$). Experimental relationships show that both Brinell Hardness (HB) and ultimate tensile strength (UTS) increased with the decrease in λ_2. The wear resistance is shown to increase with the increase in the alloy Zn content and with the decrease in λ_2. A correlation between wear, hardness and ultimate tensile strength was proposed, in which wear decreases with the increase in both HB and UTS. The observed wear mechanism is shown to be abrasive for all examined alloys and experimental conditions.

1. Introduction

The uses of aluminum alloys in industry is varied and diverse and based in important intrinsic characteristics such as weight reduction, physical-chemical properties, ease of manufacture and application to shapes and components. Such features make aluminum alloys especially interesting for use in the automotive and aeronautic industries. In addition to these features, tribological characteristics are equally important. Despite several applications of aluminum alloys in engineering, most of these alloys are utilized in the wrought condition due to their better mechanical and physical-chemical responses. However, the requirement to reduce energy consumption in the manufacturing processes has enlarged the attention concerning the use of components and parts in the as-cast condition, decreasing manufacturing steps and production costs.

Many studies have reported the effect of as-cast structures, such as grain size, columnar and equiaxed structures, the presence of intermetallic/precipitate particles, and cellular and dendrite microstructures, on the mechanical properties, mainly in aluminum-based alloys [1–6]. The tribological aspects are also investigated, specialty to establish correlations between microstructure features, solidification conditions and wear characteristics. Many researches are concentrated on anti-friction binary alloy systems, as Al-Pb, Al-Bi, Al-Sn and Al-Sb, while other are focused on ternary and quaternary systems, as Al-Pb-Cu, Al-Pb-Sn-Cu, Al-Pb-Sn-Si [7–9]. In the case of pure aluminum, the wear resistance increases with decrease in grain size and with increase in hardness, following the Hall-Petch equation [10]. With the absence of second phases, the main mechanism permitting the mechanical strength to be enhanced is that associated with the increase in density of grain boundaries, which act as barriers to the dislocation motion during plastic deformation. To obtain additional mechanical strength for pure metals, different microstructural refinement techniques are being used to produce nanoscale structures, as the production of thin films by radio frequency magnetron sputtering [11], and the

* Corresponding author.
E-mail address: carlos.santos@pucrs.br (C.A. dos Santos).

https://doi.org/10.1016/j.jallcom.2018.06.075
0925-8388/

Table 1
Chemical composition of the 752 and 782 alloys (wt%).

Alloys	Zn	Mg	Cu	Mn	Fe	Cr	Ni	Si	Al
752	5.03	2.03	0.006	0.010	0.15	0.01	0.0021	0.07	Balance
782	8.17	2.08	0.003	0.007	0.16	0.01	0.0049	0.06	Balance

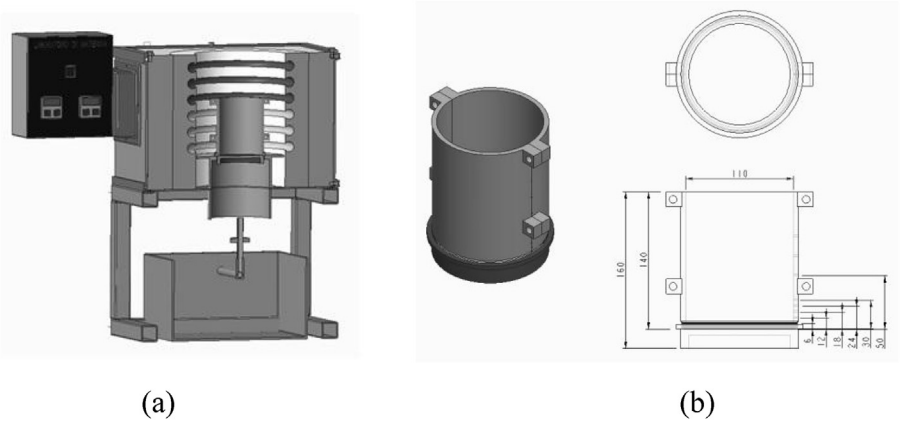

Fig. 1. Schematic representation of: (a) unidirectional furnace; and (b) metallic mold.

development of materials by hot isostatic pressing of metallic powders subjected to severe plastic deformation by high-energy ball milling process [12,13]. In the case of alloys, the wear behavior depends on the refinement of the structure and on the presence of second phases and/or particles in the interdendritic or interphase regions. When hard particles are present in the interdendritic regions, the refinement of the dendritic arm spacing improves the wear resistance. In contrast, in the case of soft particles, as bigger and more concentrated the softer particles in the interdendritic areas, better is the wear resistance. In these cases, the wear behavior is associated with the characteristics of the interdendritic phases distributed throughout the microstructure, mainly when considering reinforcement and anti-friction phases [14–17].

To reduce manufacturing steps, additive manufacturing techniques by selective laser sintering or melting (SLS/SLM) of metal powders have attracted the interest of researchers and manufacturers in recent years [18]. These processes permit near-net-shape 3D parts with complex geometry to be obtained with lower costs, higher flexibility, with the desired features located along different regions of the components. However, aspects related to the microstructure formation and the resulting mechanical properties due to the layer-by-layer method are still in progress, mainly when considering the conditions of solidification during the metal printing process. The most common alloys processed by SLM are pure iron, stainless steel, tool steels, and non-ferrous alloys such as titanium, nickel, cobalt and aluminum base alloys [19]. Despite the problems related to processing aluminum alloys by SLM, such as high reflectivity, high surface oxide film formation and high tendency to crack formation, researches have shown promising results with Al-Si and Al-Si-composites alloys [20–22], correlating the microstructure with mechanical properties, wear and corrosion

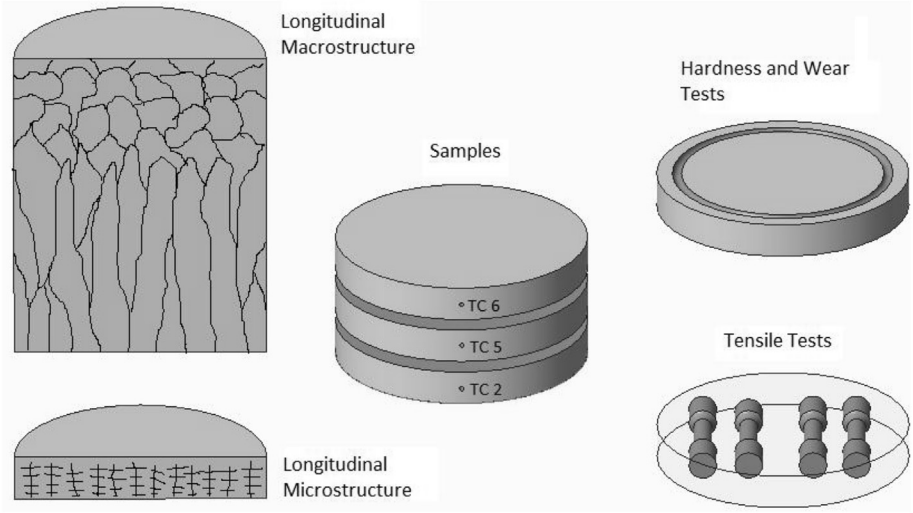

Fig. 2. Schematic representation of the directionally solidified ingot and samples/specimens extracted for metallography and mechanical testing.

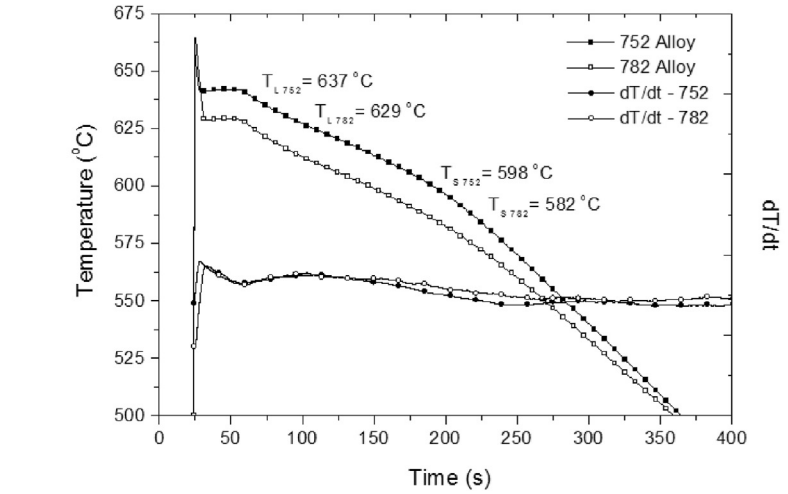

(a)

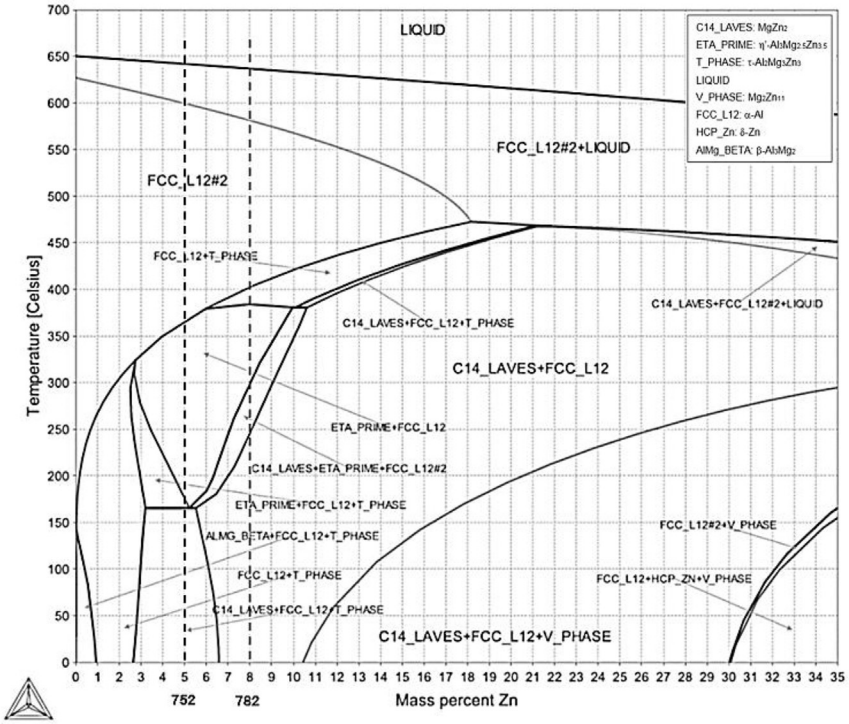

(b)

Fig. 3. (a) Experimental cooling curves, and (b) Al-2wt%Mg-Zn partial pseudo-binary diagram calculated by a computational thermodynamics software.

resistances. The refined structure obtained with these alloys using the SLM process has improved the aforementioned aspects, strengthening the importance of understanding the relationship between solidification conditions, microstructure formation and final properties. Nowadays, the challenge is to spread on this process to other aluminum-based alloys, in special for Al-Zn-Mg alloys, due to their high strength, age-hardening ability and engineering applications [23–25].

Although there are studies on wear characteristics of Al-based alloys, the lack of information regarding as-cast Al-Zn-Mg alloys with different Zn contents, and the possibility of replacing wrought alloys containing copper by as-cast alloys without copper, permitting cost reduction and enhanced mechanical properties, have motivated the present study. The present work aims to evaluate the effects of Zn additions to an Al-2wt%Mg alloy on the as-cast microstructures, mechanical properties (hardness, tensile strength) and dry sliding wear behavior. Relationships between microstructure features, mechanical properties and wear characteristics are envisaged.

2. Experimental procedure

The Al-Mg-Zn alloys were prepared using commercially pure aluminum (>99.5% purity), pure zinc (>99.7% purity) and pure magnesium (>99.9% purity), which were melted into a silicon carbide crucible covered with a boron nitrite coating and using an electric resistance furnace (melt temperature about 740 °C). After melting, samples were extracted to confirm the alloys chemical

compositions by optical emission spectrometry (OES). The average values of six measurements in each alloy, labeled as 752 and 782, are shown in Table 1. Thermal analyses by CCA (Cooling Curve Analyzes) were carried out to determining the Liquidus (T_L) and Solidus (T_S) transformation temperatures of each alloy.

An electric resistance vertical furnace having two heating zones independently controlled (Fig. 1a), was used for the unidirectional solidification experiments. A SAE 1020 steel mold, containing the molten alloy, was cooled at the bottom by a water flow rate of about 15 ± 0.1 L/min (Fig. 1b), thus permitting upward directionally solidified castings to be obtained. Type K thermocouples (1.6 mm diameter) located at different positions in the casting with respect to the bottom of the mold (Fig. 1b) were used to monitor the thermal responses during solidification by a data acquisition system. For each alloy, two identical solidified ingots (height: 75 mm – diameter: 110 mm, weight: 1.9 kg) were obtained: one for thermal

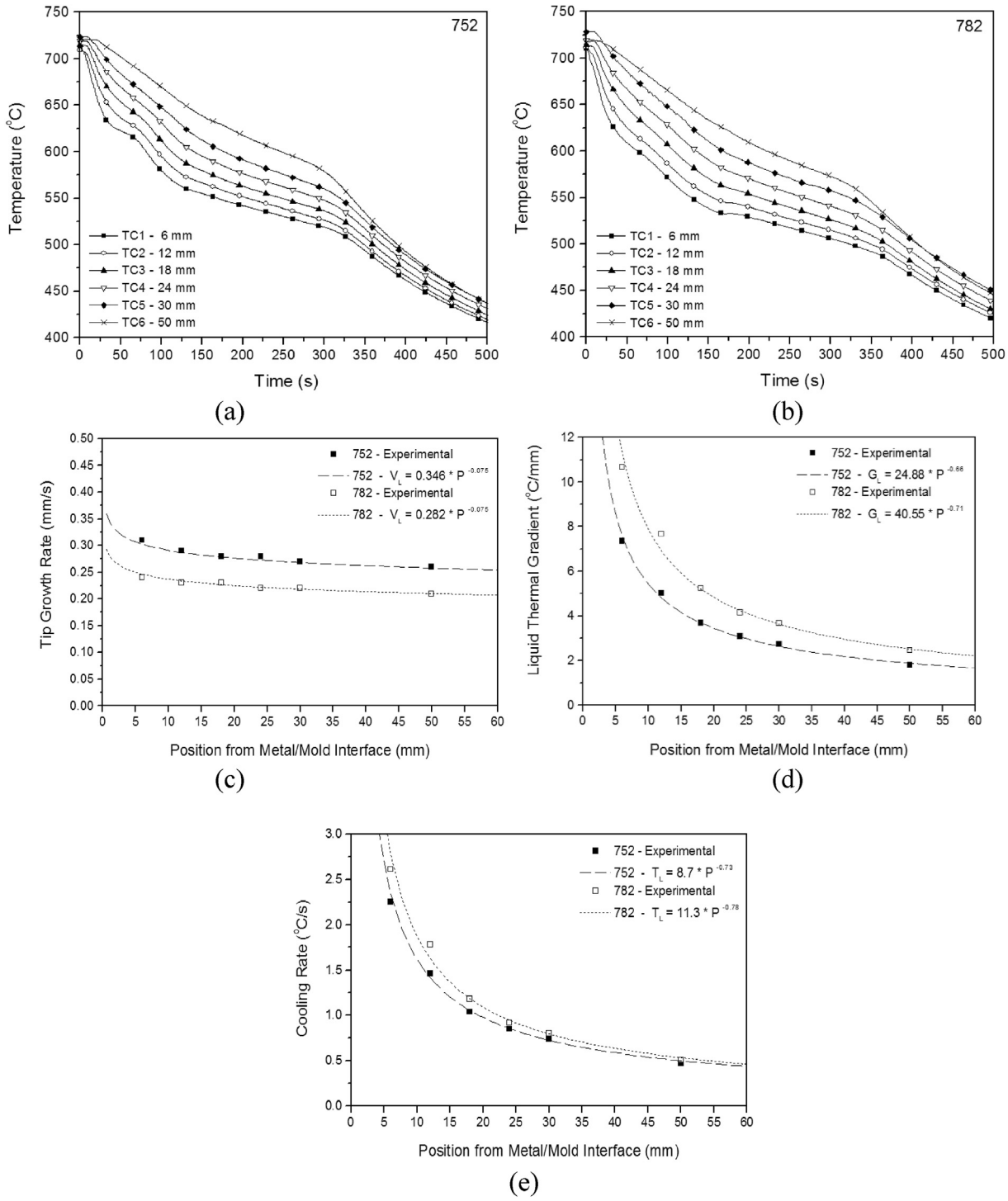

Fig. 4. (a, b) Cooling curves of the 752 and 782 alloys, (c) tip growth rate - V_L, (d) liquid thermal gradient – G_L, and (e) tip cooling rate - $\dot{T}$ as a function position along the length of the directionally solidified ingots.

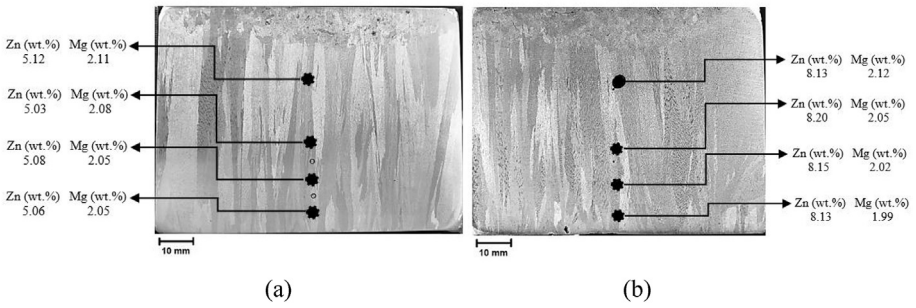

Fig. 5. Macrostructures and chemical compositions along the length of the: (a) 752, and (b) 782 alloys ingots.

and metallographic analyzes, and one for mechanical testing. For both alloys, the cooling system was started when the melt achieved a temperature at about 720 °C.

The solidified ingots were cut into longitudinal and transversal sections to extract samples for chemical and microstructural characterization by optical microscopy (OM), scanning electron microscopy (SEM), energy dispersive X-ray spectroscopy (EDS), X-ray diffraction (XRD) and appropriate specimens to undergo mechanical tests such as hardness, microhardness, tensile and wear testing, as recommended by ASTM E 10, ASTM E 384, ASTM E 8, and ASTM G 99 Standard Test Methods [26–29].

For macrostructural analyzes, the modified Keller's reagent (10% HF, 60% HCl, 20% HNO_3 and remaining distilled water) was used for etching, whereas the fluoride acid (5% HF in distilled water) was

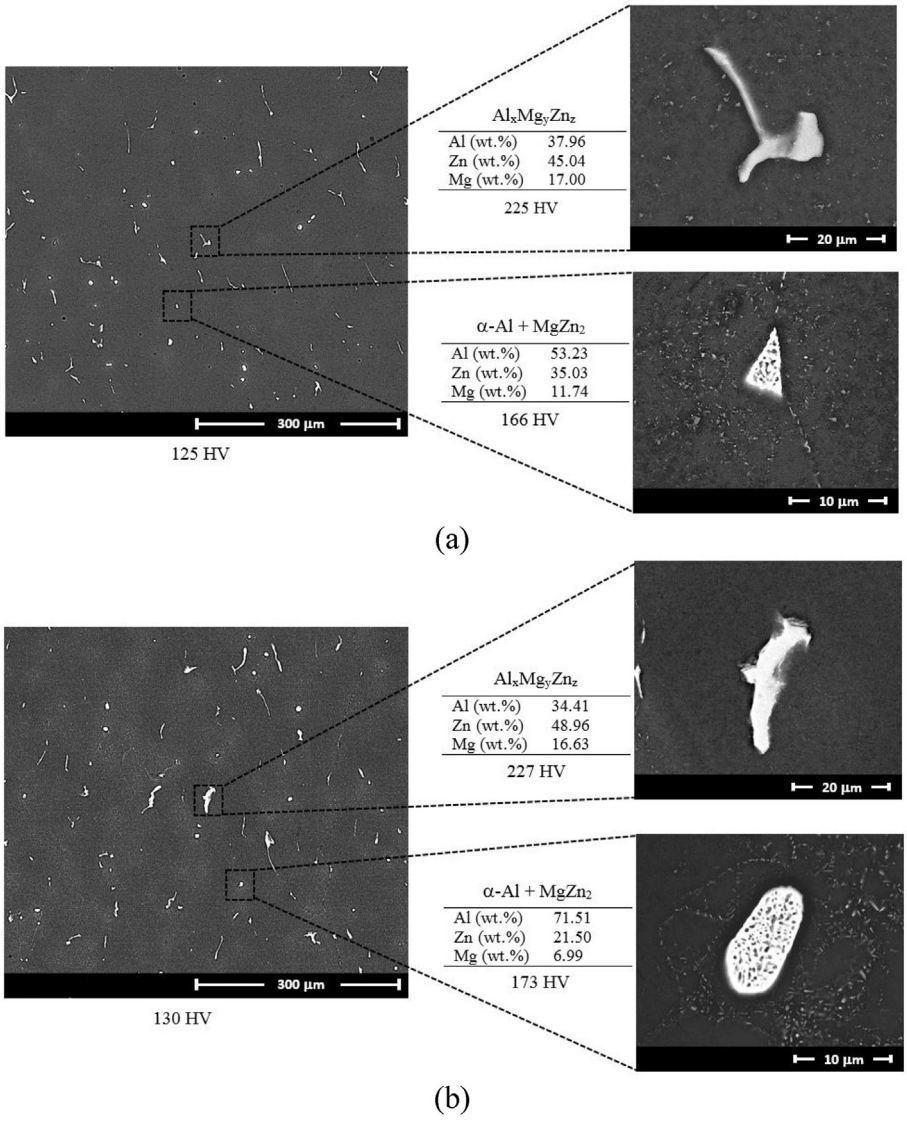

Fig. 6. SEM images and EDS analyses of: (a) 752 and (b) 782 alloys microstructures of longitudinal section of samples at 6 mm from the bottom of the casting.

used for revealing the microstructure using standard metallographic techniques [30,31]. Fig. 2 shows a schematic representation of the directionally solidified ingot with indications of samples for metallography, and specimens extracted for mechanical testing.

For hardness and wear tests, 20 mm thick discs were cut from transverse sections of the directionally solidified ingots. Brinell hardness measurements were made on both faces of the discs (five measurements for each face), and Vickers microhardness tests were performed on both the matrix and the phases of the alloys. After that, the pin-on-disc method, as suggested by the ASTM G99 Standard [29], was used to simulate wear tests under dry sliding contact. Alumina ceramic balls (>96% Al_2O_3 – 1500 HV) with a diameter of 10-mm were used, because there was no metallurgical compatibility between the pin and the discs [32]. The applied load was 14.7 N at 1.8 m/s sliding speed and 1000 m of total sliding distance for all tests carried out. Before wear tests, the discs were machined to a 112 mm diameter and ground on both faces with #100, #220, #320, #400, #600, and #1200 sandpapers, resulting in a superficial roughness <0.8 mm. Both faces were dedicated to tests. Before each test, the discs were cleaned in an ultrasonic bath for 10 min using ethanol, and then dried using a hand-held hot-air device. The wear track width (mm) and volume loss (mm^3) were analyzed for each 100 m of sliding distance, at 8 locations positioned 45° from each other. All wear-track widths were examined using an optical microscope with a 0.01 mm resolution measurement system. The disc volume loss (V_{disc}) and the wear coefficient (k) were determined using Equation (1) [29] and the Archard Equation (2) [33,34], as given by:

$$V_{disc} = 2\cdot\pi\cdot R\left[r^2\cdot \text{sen}^{-1}\left(\frac{w}{2\cdot r}\right) - \frac{w}{4}\left(4\cdot r^2 - w^2\right)^{\frac{1}{2}}\right] \qquad \left(mm^3\right) \tag{1}$$

$$\frac{V_{disc}}{S} = \frac{k\cdot L}{H} \qquad \left(mm^3/N\cdot m\right) \tag{2}$$

where R is the wear-track radius (mm), r is the pin end radius (mm), w is the wear-track width (mm), H is the disc Brinell hardness, L is the normal applied load (kgf) and S is the sliding distance (mm). For tensile testing, four specimens were extracted from each selected transverse section, as shown in Fig. 2.

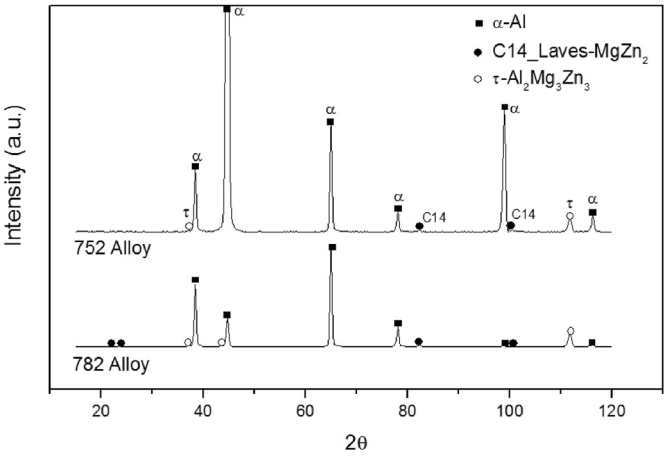

Fig. 7. XRD patterns of the 752 and 782 alloys.

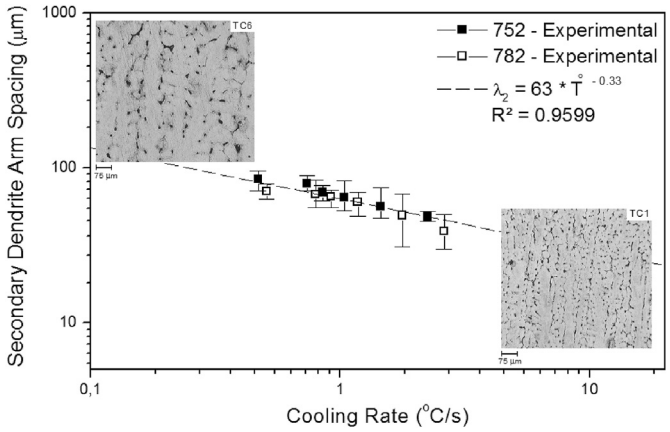

Fig. 8. Evolution of the secondary dendrite arm spacing (λ_2) as a function of cooling rate along the length of the 752 and 782 alloys ingots. R^2 is the coefficient of determination.

3. Results and discussion

3.1. Solidification and structures

Thermal analyzes were performed with each examined alloy to obtain cooling curves near to equilibrium conditions with a view to permitting the *Liquidus* and *Solidus* temperatures of each alloy to be determined. The alloys were poured into a special rectangular sand mold (25 mm × 25 mm × 75 mm), which permits low cooling rates (<15 °C/min) to be attained during solidification. The temperatures corresponding to the solidification range of the alloys are shown in Fig. 3a. For the 752 alloy, the *Liquidus* temperature (T_L) was determined at 637 °C (e) and the *Solidus* temperature (T_S) at 598 °C, while the 782 alloy had the experimental value of T_L at 629 °C and that of T_S at 582 °C. These values agree with those observed in the study reported by Acer et al. [35] with an Al-5.5 wt%Zn-2.5 wt%Mg alloy. Simulations were also performed using a computational thermodynamics software to determine the Al-2wt%Mg-Zn pseudo-binary phase diagram, as shown in Fig. 3b. The results of T_L and T_S for the 5 wt%Zn and 8 wt%Zn in Fig. 3b are quite close to those experimentally determined, and the slight differences may be attributed to the trace elements in the composition of both alloys, as shown in Table 1.

According to the calculated Al-2wt%Mg-Zn pseudo-binary phase diagram, the solidification path of the 752 Alloy is: L → (α-Al + L) → (α-Al) → (α-Al + η′-$Al_3Mg_{2.5}Zn_{3.5}$) → (α-Al + η′-$Al_3Mg_{2.5}Zn_{3.5}$ + τ-$Al_2Mg_3Zn_3$) → (α-Al + τ-$Al_2Mg_3Zn_3$ + C14-LAVES: $MgZn_2$), while the 782 Alloys presents the following solidification path: L → (α-Al + L) → (α-Al) → (α-Al + τ-$Al_2Mg_3Zn_3$) → (α-Al + η′-$Al_3Mg_{2.5}Zn_{3.5}$) → (α-Al + η′-$Al_3Mg_{2.5}Zn_{3.5}$ + C14-LAVES: $MgZn_2$) → (α-Al + C14-LAVES: $MgZn_2$).

The cooling curves acquired during upward unidirectional solidification of the 752 and 782 alloys ingots are shown in Fig. 4a and b. They represent the thermal evolution at six specific positions along the length of the ingot where the thermocouples (TC) were strategically located at different positions (P) from the cooled bottom (TC1 - 6 mm, TC2 - 12 mm, TC3 - 18 mm, TC4 - 24 mm, TC5 - 30 mm, TC6 - 50 mm). Using the cooling profiles, solidification thermal parameters as solidification velocity or tip growth rate (V_L), liquid temperature gradient (G_L) and tip cooling rate ($\dot{T}$) were determined. V_L was calculated by the dP/dt derivative of a P = f(t) function, which is determined by considering the time (t) associated with the passage of the *Liquidus* isotherm by each thermocouple position (P), G_L by the relation between the tip growth rate

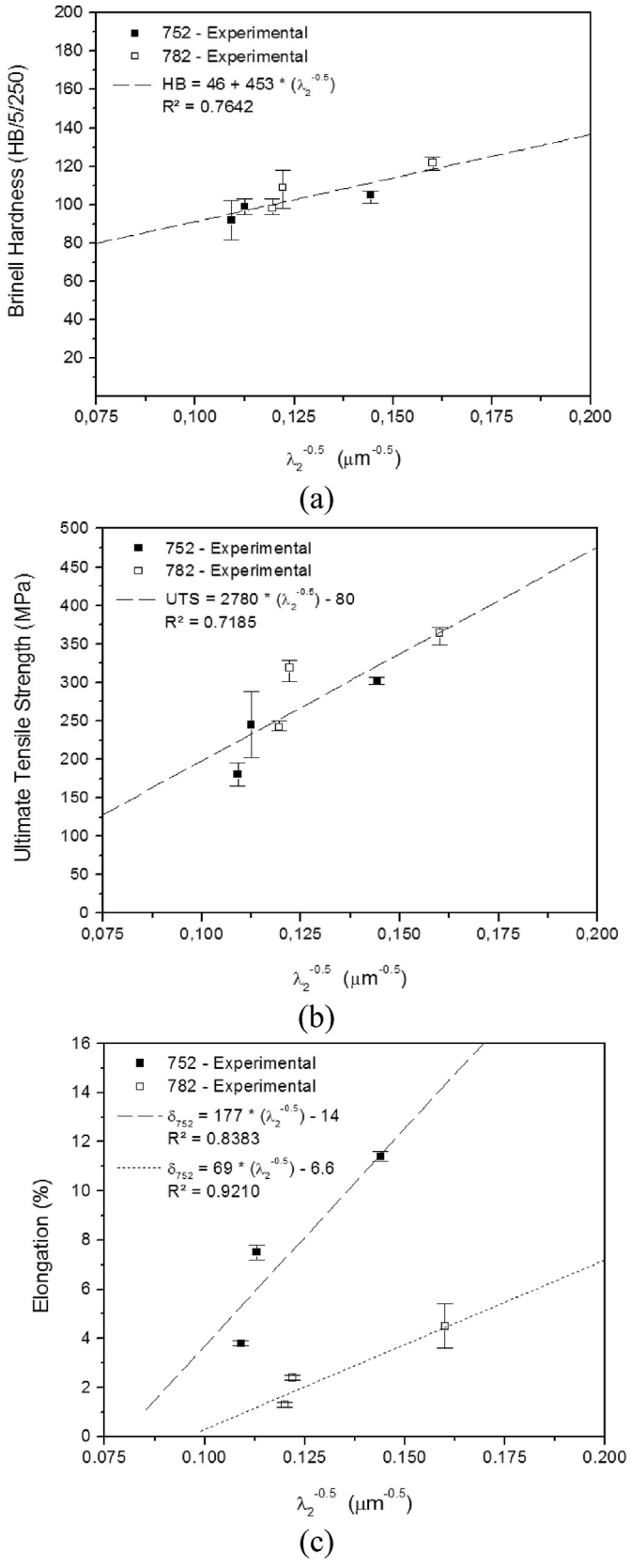

Fig. 9. (a) Brinell hardness, (b) ultimate tensile strength, and (c) elongation as a function of secondary dendrite arm spacing (λ_2) along the length of the of the 752 and 782 alloys ingots. R^2 is the coefficient of determination.

and cooling rate ($G_L = \dot{T}/V_L$), and $\dot{T}$ by the time-derivative of the cooling curve (dT/dt) immediately ahead the *Liquidus* temperature. Experimental expressions were obtained for $V_L = f(P)$, $G_L = f(P)$ and $\dot{T} = f(P)$, as shown in Fig. 4c, d and e.

As can be observed in Fig. 4, the solidification conditions for the 752 alloy indicated higher tip growth rates and slightly lower tip cooling rates profiles as compared to the corresponding values of the 782 alloy. This demonstrates that the increase in the alloy Zn content does not induce significant differences in the cooling rate profiles, which are very close for both alloys. For transient solidification conditions the cooling rate synthesizes the thermal gradient (G_L) and the growth rate (V_L), which are interdependent and vary freely in time, that is $\dot{T} = (G_L V_L)$. If the growth rate profile is lower for the 782 alloy, due to lower *Liquidus* temperature and differences in thermophysical properties, then the G_L profile of such alloy has to be higher than that of the 752 alloy, thus making the cooling rates profiles of both alloys to be quite close, as shown in Fig. 4e.

The solidification macrostructures of the ingots are presented in Fig. 5, and it can be observed they are predominantly columnar in the regions where the thermocouples were positioned, with the grains aligned along the heat flow path. The chemical composition using OES analyzes performed on each position along the ingots have demonstrated that Zn and Mg content variation is insignificant (<2%). For the 752 alloy (Fig. 5a), a columnar to equiaxed transition is noted at approximately 70 mm from the metal/mold interface. An aligned columnar structure is also observed for the 782 alloy (Fig. 5b), and the columnar to equiaxed transition occurred about 65 mm from the bottom of the ingot. Finer grains are observed as compared to those of the 752 alloy. This seems to occur due to the higher Zn content of the 758 alloy, which favors structure refining and columnar-to-equiaxed transition [36–39].

Scanning electron microscopy (SEM) and energy dispersive X-ray spectroscopy (EDS) were used to identify the phases and precipitates on both alloys. Fig. 6a presents the results obtained for the 752 alloy, where it is possible to identify the α-aluminum matrix (grey areas), and two precipitates (white areas). According to Lim et al. [40] and Raghavan [41], these precipitates in the as-cast microstructures are the intermetallics C14-LAVES ($MgZn_2$) and τ ($Al_2Mg_3Zn_3$). Vickers microhardnesses of matrix and precipitates are also indicated in Fig. 6. The equilibrium phase diagram of Fig. 3b indicates the presence of the α-Al + τ phase + C14-LAVES phase at 25 °C. However, similar analyzes for the 782 alloy (Fig. 6b) have permitted to identify the same precipitates, although the equilibrium phase diagram does not indicate the presence of the τ phase at 25 °C, and this seems to be caused by the non-equilibrium solidification conditions of the experiments of the present study. In both alloys, an interdendritic mixture composed of α-Al + $MgZn_2$ can be observed (bottom right-side images), which is in agreement with the results reported by Acer et al. [35]. A visual comparison shows that the size and distribution of $MgZn_2$ and $Al_2Mg_3Zn_3$ precipitates increased with the increase in the Zinc content, as well as with the distance from the heat-extracting surface of the castings (bottom of the casting). As seen in Fig. 6, the shape of the τ precipitate is predominantly irregular and faceted, while the α-Al + $MgZn_2$ microconstituent consists in an intermixed network.

Fig. 7 shows the XRD patterns of the 752 and 782 alloys. The results confirm that the microstructures of both alloys consist of an α-aluminum matrix (face-centered cubic crystal structure) with $MgZn_2$ (hexagonal crystal structure) and $Al_2Mg_3Zn_3$ (cubic crystal structure) precipitates. As the alloy Zn content increases, the volume fraction of the $MgZn_2$ phase increases, while the $Al_2Mg_3Zn_3$ phase increases with the increase in the Mg content. These results agree with those reported in the literature for Al-Zn-Mg alloys with different Zn and Mg contents [42–45].

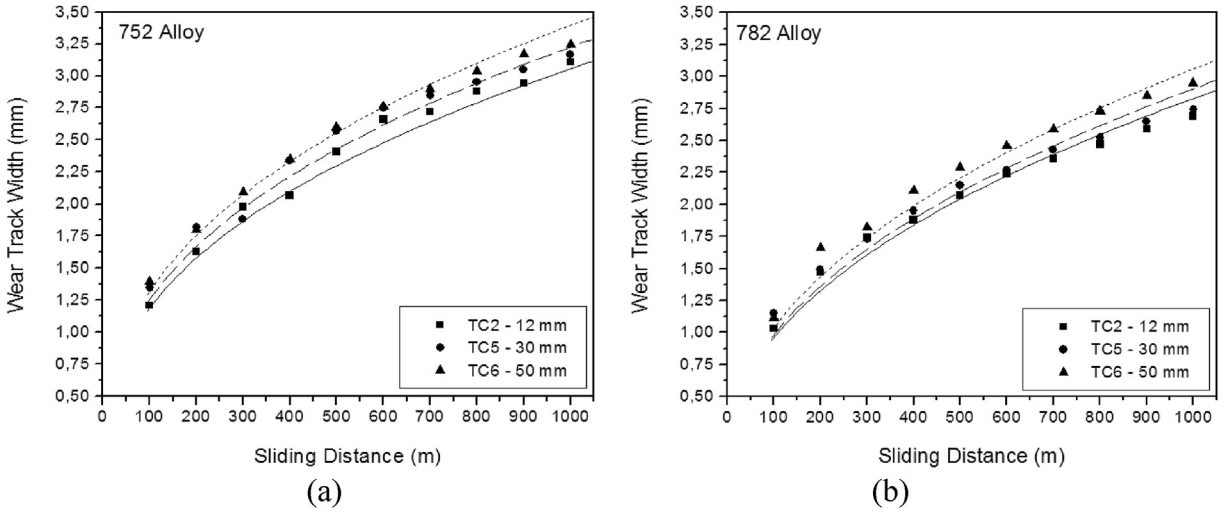

Fig. 10. Wear-track width as a function of sliding distance of: (a) 752, and (b) 782 alloys samples.

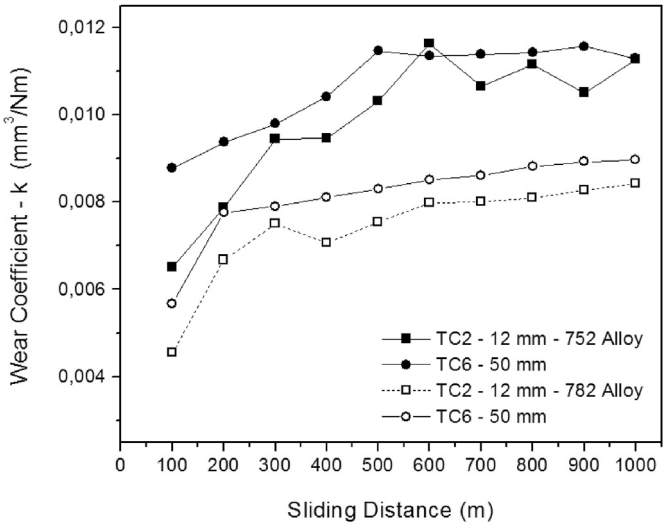

Fig. 11. Comparison of the wear coefficient as a function of sliding distance at 12 mm and 50 mm distance from metal/mold interface for both examined alloys ingots.

An α-Al matrix having a predominant dendritic morphology can be observed along the length of both alloys ingots. The secondary dendrite arm spacings (λ_2) were measured using a specific software coupled with an optical microscope (20 measurements for each position), and the results as a function of the tip cooling rate ($\dot{T}$) are presented in Fig. 8. The microstructures corresponding to the thermocouple positions (TC1 − 6 mm and TC6 − 50 mm) are also shown inside the graph. The experimental results are represented by the points, and the best fitted curve to the experimental points has been obtained by regression analysis and is represented by the dashed line. As can be observed, λ_2 increases with the decrease in $\dot{T}$ for both alloys, and the experimental trend of both alloys can be expressed by a single equation.

3.2. Mechanical properties

The results of tensile and hardness tests are presented in Fig. 9. Fig. 9a shows Brinell hardness (HB) variation as a function of the secondary dendrite arm spacing (λ_2) along the length of the 752 and 782 alloys ingots. It can be seen that HB decreases from the cooled bottom toward the top of the directionally solidified ingots, that is the lower λ_2 the higher HB. Similar behavior is associated

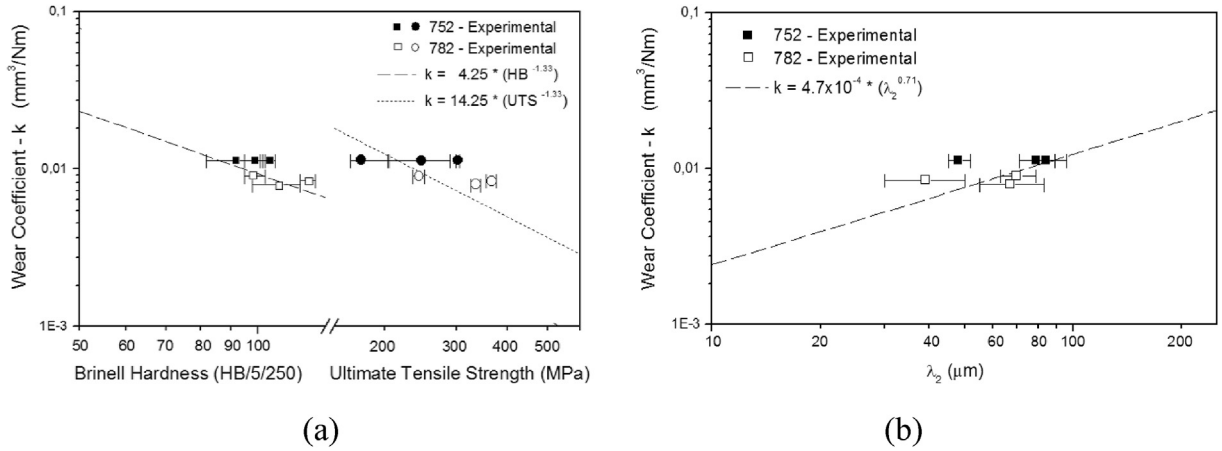

Fig. 12. (a) Wear coefficients as a function of: (a) Brinell hardness (HB) and ultimate tensile strength (UTS); and (b) secondary dendrite arm spacing (λ_2).

with the ultimate tensile strength (Fig. 9b). The alloys ductility, represented by the elongation to fracture, have also a similar trend, with the elongation increasing with the decrease in λ_2 (Fig. 9c). However, the 752 and 782 alloys showed different tendencies, with the former exhibiting higher ductility for a given value of λ_2, that is, the increase in the alloy Zn content is shown to be detrimental to ductility. This seems to be associated with the increase in the volume fraction of the $MgZn_2$ phase, which increases with the increase in the alloy Zn content. In general, the increase in hardness and strength values is caused by the refinement of the dendritic array and is strongly linked to the more homogeneous distribution of second phases and other obstacles in the interdendritic regions to the displacement of dislocations during the slip process of the dendritic matrix, mainly in the as-cast non-ferrous alloys [46–56]. The ultimate tensile strength and hardness values obtained for both alloys are quite superior to those reported in the study by Acer and collaborators [57] with an Al-5.5Zn-2.5 Mg alloy in the as-cast condition, mainly when considering higher Zn content that increases the volume fraction of the $MgZn_2$ phase and induces an interdendritic refinement, as discussed in section 3.1. In comparison with alloys containing Cu, the results are moderately smaller than those reported by Isadare et al. [58] for a 7075 alloy in the as-cast condition. However, when considered the 782 alloy, the results obtained in the present work are similar to those in the annealing condition. This indicates that the 782 alloy can be used to replace alloys with Cu addition in some applications, in special when the solidification conditions can be programmed with a view to permitting refined microstructures to be obtained. The equations presented in Figs. 8 and 9 can be applied to estimate these mechanical properties as a function of the secondary dendrite arm spacing and cooling rates, following the formalism presented by the Hall-Petch equation.

Fig. 10 shows wear-track width for both alloys until 1000 m sliding distance. The maximum Hertzian contact pressure calculated considering the elastic modulus and Poisson's ratio of the alloys ($E = 70$ GPa and $\nu = 0.32$) is 780 MPa, which is higher than the yield strength of the materials in the as-cast condition. Despite the much higher hardness of the alumina pin as compared to that of the examined alloys discs, material transfer from the pin to the discs has not been observed in all tests. The wear-track width indicates better wear resistance for positions near to metal/mold interface where the as-cast microstructure is more refined, and consequently harder and stronger. When both alloys are compared, the 752 alloy presented higher values than those of the 782 alloy.

The wear coefficients (k) are presented in Fig. 11. For the first 200 m sliding distance, an initial transient wear regime has been noted for the 782 alloy, and after that a steady-state was achieved, while the 752 alloy showed the transient/steady-state behavior transition after 600 m sliding distance. According to Rao et al. [24,25], at an initial stage, wear is essentially caused by fragmentation of surface asperities and removal of material from the softer matrix by abrasion. As the sliding distance increases, the surface deformation also increases, and consequently, the subsurface strain hardening protects the material and promotes decrease in the wear rate. As shown in Fig. 11, the wear coefficients for the 752 alloy indicated poorer wear behavior as compared to that of the 782 alloy, for samples of all examined positions. The wear coefficient for the 752 alloy varied from 6.3×10^{-3} to 11.2×10^{-3} mm^3/Nm, while the 782 alloy presented values in the 4.4×10^{-3} to 8.9×10^{-3} mm^3/Nm range.

3.3. Relations between wear, mechanical properties and microstructures

With the wear-coefficient (k) as a function of sliding distance, it was possible to establish relationships of k with hardness, ultimate tensile strength and secondary dendrite arm spacing, as shown in Fig. 12. In this study, it was found a direct correlation between wear and hardness and ultimate tensile strength, where wear decreases with the increase in both HB and UTS. A -1.33 power law coefficient characterized the wear coefficients as a function of hardness and ultimate tensile strength for both alloys, and a 0.71 power law when related to the secondary dendrite arm spacing.

When comparing the 782 alloy to the 752 alloy, it can be observed smaller wear for the samples of a position closer to the cooled bottom of the ingots (TC2-12 mm), which is associated with smaller dendritic spacings, and as consequence with higher hardness and ultimate tensile strength. This indicates that the microstructure has a strong influence on the wear behavior and is due to higher Zn content and the higher amount of $MgZn_2$ precipitate that is harder (~170 HV) than α-aluminum matrix (~130 HV), and helps to protect the surface of the material.

Fig. 13a presents the variation of wear volume loss as a function of sliding distance for both alloys in the analyzed positions. It can be

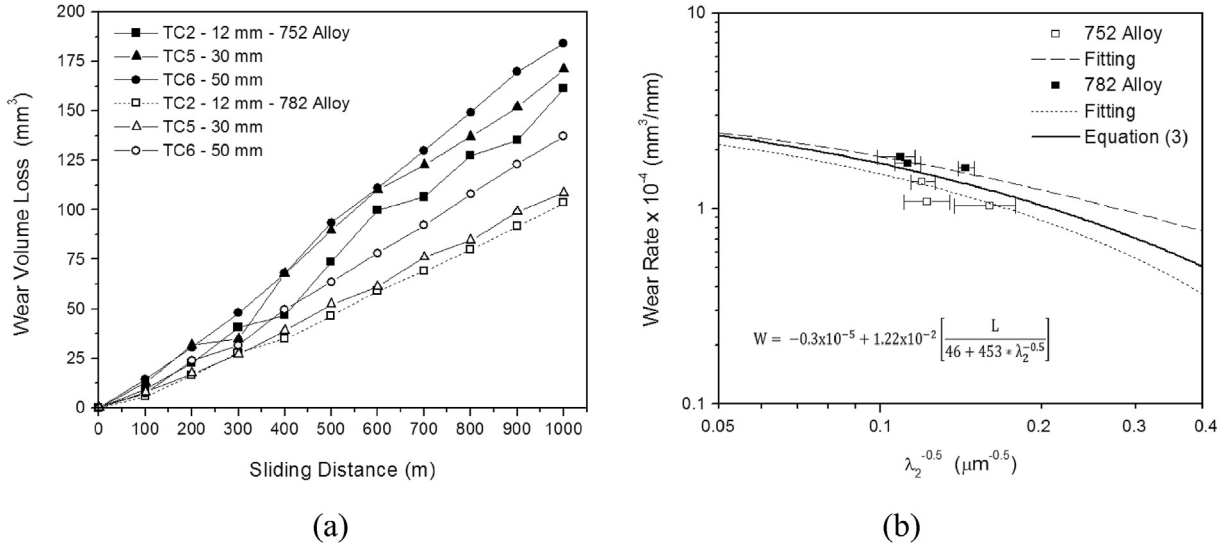

Fig. 13. (a) Wear volume loss as a function of sliding distance, (b) Wear rate as a function of the reciprocal square root of the secondary dendrite arm spacing ($\lambda_2^{-0.5}$).

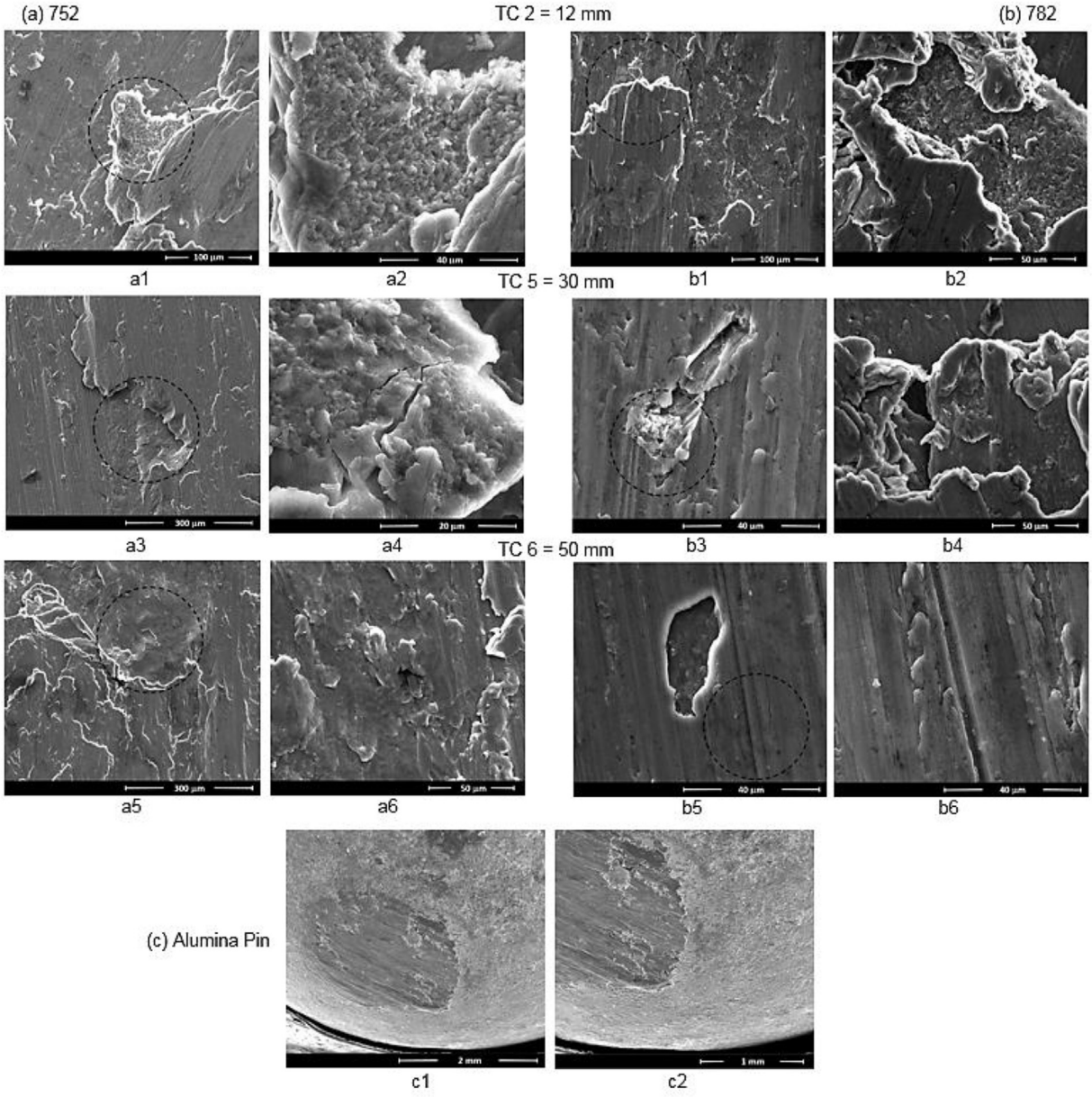

Fig. 14. Wear-track surfaces of the: (a) 752 alloy, (b) 782 alloy, and (c) the alumina-pin surface.

observed that the wear volume loss increases at an almost constant rate, and the volume loss of the 752 alloy is significantly higher than that of the 782 alloy. With these values, and based on the approach proposed by Prasada Rao [10] and Farhat [11] using the Archard's wear model [33], the equation presented in Fig. 12a can be rearranged to express the wear rate (W) as a function of the wear coefficient (k) and secondary arm dendrite spacing (λ_2) in the format of a Hall-Petch equation, as follows:

$$W = W_o + k\left\{\frac{L}{[46 + 453^*(\lambda 2^{-0.5})]}\right\} \qquad \left(\mathrm{mm}^3/\mathrm{mm}\right) \qquad (3)$$

From Equation (3), it can be seen that the wear rate is inversely proportional to hardness and directly proportional to k and λ_2. It can be seen that with the refinement of the secondary arm dendrite spacing (λ_2), the wear rate decreases. A comparison between experimental and calculated values is shown in Fig. 13b. The horizontal error bars represent the variation in λ_2, and the dashed and dotted lines represent the experimental evolutions of wear rates of the 752 and 782 alloys, respectively, while the solid line represents the evolution of wear rate given by Eq. (3). The results suggest that the wear rate of the examined alloys can be described by this equation considering the experimental wear conditions of the present study.

Fig. 14 shows the wear-track surfaces analyzed by SEM for the 752 and 782 alloys, as well as the alumina-pin surface. The 752 alloy presented more areas in which material was removed from the surface (large craters) as compared to the 782 alloy. Delamination, scratches, and debris were also observed to be more severe for the 752 alloy samples (a1-c4). The 782 alloy demonstrated the presence of small craters, mild grooves, and micro cuts (b1-b4). Analyzing the wear-track surfaces and correlating with the wear-track widths, wear coefficients and wear rates, the 752 alloy exhibited more severe wear than that of the 782 alloy. This was

probably due to its microstructure, which was composed of higher secondary dendrite arm spacing and higher ductility, facilitating the removal of material. Aluminum alloys typically display the formation of an oxide layer on the surface, which influences the wear behavior [59,60]. The superficial and sub-superficial plastic deformation contributes to the strain hardening of the material, and when a critical level is achieved, fragmentation and debris formation occurs, as shown in Fig.14 a4, mainly in the oxide layer. The addition of Zn to the Al-2wt%Mg alloy has induced a tendency to increase the wear resistance due to both increase in solid solution strengthening of the matrix and hard particles precipitation. These hard particles, when uniformly distributed and associated with a hard matrix, help to protect the material surface against wear. However, an opposite behavior can be observed if the matrix has lower hardness, and the particles can plow the material of the matrix. As there is not metallurgical compatibility between the pin and the disc, adhesive wear was not observed in all examined conditions, and abrasive wear was the predominant wear mechanism. This can be confirmed by a strong presence of delamination, grooves and scuffing.

4. Conclusions

Based on the results obtained, the following major conclusions can be drawn from the present experimental study:

- An experimental equation was derived relating the secondary dendrite arm spacing (λ_2) to the solidification cooling rate ($\dot{T}$), in which λ_2 decreases with the increase in $\dot{T}$. The experimental trend of both alloys was shown to be expressed by a single equation.
- The Brinell hardness (HB) and the ultimate tensile strength (UTS) were related to λ_2 by experimental relationships that were developed from the experimental scatter. It was observed that both HB and UTS increased with the decrease in λ_2 for all conditions experimentally examined, and that single equations are able to represent the evolution of HB vs. λ_2 and UTS vs. λ_2 for both examined alloys. However, the 752 and 782 alloys showed different tendencies with regard to the evolution of the elongation to fracture versus λ_2, with the former exhibiting higher ductility for a given value of λ_2, that is, the increase in the alloy Zn content is shown to be detrimental to ductility. This seems to be associated with the corresponding increase in the volume fraction of the $MgZn_2$ phase for the 782 alloy.
- The 752 alloy was shown to have a poorer wear behavior in terms of wear-track width and wear coefficient as compared to the 782 alloy, probably due its higher ductility and coarser microstructure.
- The wear-track surfaces indicated that the 752 alloy had more severe wear as compared to that of the 782 alloy.
- A correlation between wear, hardness and ultimate tensile strength was proposed, in which the wear decreases with the increase in these mechanical properties.
- Abrasive wear was observed for both alloys and at all conditions experimentally examined.

Acknowledgements

The authors acknowledge the support provided by CNPq (The Brazilian Research Council – grant number 403303/2016-8; 301600/2015-5), FAPERGS (The Scientific Research Foundation of the State of Rio Grande do Sul) and PUCRS (Pontifical Catholic University of Rio Grande do Sul).

References

[1] C. Brito, G. Reinhart, H. Nguyen-Thi, N. Mangelinck-Noël, N. Cheung, J.E. Spinelli, A. Garcia, High cooling rate cells, dendrites, microstructural spacings and microhardness in a directionally solidified Al-Mg-Si alloy, J. Alloys Compd. 636 (2015) 145–149.
[2] F. Bertelli, C. Brito, I.L. Ferreira, G. Reinhart, H. Nguyen-Thi, N. Mangelinck-Noël, N. Cheung, A. Garcia, Cooling thermal parameters, microstructure, segregation and hardness in directionally solidified Al-Sn-(Si;Cu) alloys, Mater. Des. 72 (2015) 31–42.
[3] T.A. Costa, M. Dias, L.G. Gomes, O.L. Rocha, A. Garcia, Effect of solution time in T6 heat treatment on microstructure and hardness of a directionally solidified Al-Si-Cu alloy, J. Alloys Compd. 683 (2016) 485–494.
[4] R.V. Reyes, R. Kakitani, T.A. Costa, J.E. Spinelli, N. Cheung, A. Garcia, Cooling thermal parameters, microstructural spacing and mechanical properties in a directionally solidified hypereutectic Al-Si alloy, Phil. Mag. Lett. 96 (2016) 228–237.
[5] L.F. Gomes, B.L. Silva, A. Garcia, J.E. Spinelli, Dendritic growth, solidification thermal parameters, and Mg content affecting the tensile properties of Al-Mg-1.5 wt pct Fe alloys, Metall. Mater. Trans. A 48 (2017) 1841–1855.
[6] R.V. Reyes, T.S. Bello, R. Kakitani, T.A. Costa, A. Garcia, N. Cheung, J.E. Spinelli, Tensile properties and related microstructural aspects of hypereutectic Al-Si alloys directionally solidified under different melt superheats and transient heat flow conditions, Mater. Sci. Eng. A 685 (2017) 235–243.
[7] K. Lepper, M. James, J. Chashechkina, D.A. Rigney, Sliding behavior of selected aluminum alloys, Wear 203–204 (1997) 46–56.
[8] H.-M. Kim, T.-S. Kim, C. Suryanarayana, B.-S. Chun, Microstructure and wear characteristics of rapidly solidified Al–Pb–Cu alloys, Mater. Sci. Eng. A 287 (2000) 59–65.
[9] E.S. Freitas, A.P. Silva, J.E. Spinelli, L.C. Casteletti, A. Garcia, Inter-relation of microstructural features and dry sliding wear behavior of monotectic Al–Bi and Al–Pb alloys, Tribol. Lett. 55 (2014) 111–120.
[10] A.K. Prasada Rao, K. Das, B.S. Murty, M. Chakraborty, Effect of grain refinement on wear properties of Al and Al-7Si alloy, Wear 257 (2004) 148–153.
[11] Z.N. Farhat, Y. Ding, D.O. Northwood, A.T. Alpas, Effect of grain size on friction and wear of nanocrystalline aluminum, Mater. Sci. Eng. A 206 (1996) 302–313.
[12] Z. Wang, R.T. Qu, S. Scudino, B.A. Sun, K.G. Prashanth, D.V. Louzguine-Luzgin, M.W. Chen, Z.F. Zhang, J. Eckert, Hybrid nanostructured aluminum alloy with super-high strength, NPG Asia Mater. 7 (2015) e2291–e2298.
[13] R.K. Gupta, D. Fabijanic, T. Dorin, Y. Qiu, J.T. Wang, N. Birbilis, Simultaneous improvement in the strength and corrosion resistance of Al via high-energy ball milling and Cr alloying, Mater. Des. 84 (2015) 270–276.
[14] K.S. Cruz, E.S. Meza, F.A.P. Fernandes, J.M.V. Quaresma, L.C. Casteletti, A. Garcia, Dendritic arm spacing affecting mechanical properties and wear behavior of Al-Sn and Al-Si alloys directionally solidified under unsteady-state conditions, Metall. Mater. Trans. A 41 (2010) 972–984.
[15] E.S. Freitas, J.E. Spinelli, L.C. Casteletti, A. Garcia, Microstructure–wear behavior correlation on a directionally solidified Al–In monotectic alloy, Tribol. Int. 66 (2013) 182–186.
[16] F. Bertelli, E.S. Freitas, N. Cheung, M.A. Arenas, A. Conde, J. Damborenea, A. Garcia, Microstructures, tensile properties and wear resistance correlations on directionally solidified Al-Sn-(Cu-Si) alloys, J. Alloys Compd. 695 (2017) 3621–3631.
[17] T.A. Costa, M. Dias, E.S. Freitas, L.C. Casteletti, A. Garcia, The effect of microstructure length scale on dry sliding wear behaviour of monotectic Al-Bi-Sn alloys, J. Alloys Compd. 689 (2016) 767–776.
[18] E.O. Olakanmi, R.F. Cochrane, K.W. Dalgarno, A review on selective laser sintering/melting (SLS/SLM) of aluminum alloy powders: processing, microstructure, and properties, Prog. Mater. Sci. 74 (2015) 401–477.
[19] K.G. Prashanth, S. Scudino, H.J. Klauss, K.B. Surreddi, L. Löber, Z. Wang, A.K. Chaubey, U. Kühn, J. Eckert, Microstructure and mechanical properties of Al–12Si produced by selective laser melting: effect of heat treatment, Mater. Sci. Eng. A 590 (2014) 153–160.
[20] K.G. Prashanth, B. Debalina, Z. Wang, P.F. Gostin, A. Gebert, M. Calin, U. Kuhn, M. Kamaraj, S. Scudino, J. Eckert, Tribological and corrosion properties of Al-12Si produced by selective laser melting, J. Mater. Res. 29 (2014) 2044–2054.
[21] K.G. Prashanth, H.S. Shahabi, H. Attar, V.C. Srivastava, N. Ellendt, V. Uhlenwinkel, J. Eckert, S. Scudino, Production of high strength Al_8Nd_8-Ni_5Co_2 alloy by selective laser melting, Additi. Manuf. 6 (2015) 1–5.
[22] K.G. Prashanth, S. Scudino, A.K. Chaubey, L. Lober, H. Attar, F.P. Schimansky, F. Pyczak, J. Eckert, Processing of Al-12Si-TNM composites by selective laser melting and evaluation of compressive and wear properties, J. Mater. Res. 31 (2016) 55–65.
[23] A.F. Norman, K. Hyde, F. Costello, S. Thompson, S. Birley, P.B. Prangnell, Examination of the effect of Sc on 2000 and 7000 series aluminium alloy castings: for improvements in fusion welding, Mater. Sci. Eng. A 354 (2003) 188–198.
[24] R.N. Rao, S. Das, D.P. Mondal, G. Xixit, Dry sliding wear behaviour of cast high strength aluminium alloy (Al–Zn–Mg) and hard particle composites, Wear 267 (2009) 1688–1695.
[25] R.N. Rao, S. Das, D.P. Mondal, G. Dixit, Effect of heat treatment on the sliding wear behaviour of aluminum alloy (Al-Zn-Mg) hard particle composite, Tribol. Int. 43 (2010) 330–339.

[26] American Society for Testing and Materials, Standard Test Methods for Brinell Hardness of Metallic Materials, ASTM E 10a, ASM International, USA, 2017.
[27] American Society for Testing and Materials, Standard Test Method for Microindentation Hardness of Materials, ASTM E 384, ASM International, USA, 2017.
[28] American Society for Testing and Materials, Standard Test Methods for Tension Test of Metallic Materials, ASTM E 8, ASM International, USA, 2016.
[29] American Society for Testing and Materials, ASTM G, Standard Test Method for Wear Testing with a Pin-on-disk Apparatus, vol. 99, ASM International, USA, 2004.
[30] American Society for Testing and Materials, Standard Guide for Preparation of Metallographic Specimens, ASTM E 3, ASTM International, USA, 2017.
[31] American Society for Testing and Materials, Standard Practice for Microetching Metals and Alloys, ASTM E 407, ASM International, USA, 2015.
[32] M. Hua, X. Wei, J. Li, Friction and wear behavior of SUS 304 austenitic stainless steel against Al_2O_3 ceramic ball under relative high load, Wear 265 (2008) 799–810.
[33] J.F. Archard, Contact and rubbing of flat surfaces, J. Appl. Phys. 24 (1953) 981–988.
[34] J.K. Lancaster, Material-specific wear mechanism: relevance to wear modelling, Wear 141 (1990) 159–183.
[35] E. Acer, E. Çadırlı, H. Erol, T. Kırındı, M. Gündüz, Effect of heat treatment on the microstructures and mechanical properties of Al-5.5Zn-2.5Mg alloy, Mater. Sci. Eng. A 662 (2016) 144–156.
[36] C.A. Siqueira, N. Cheung, A. Garcia, Solidification thermal parameters affecting the columnar-to-equiaxed transition, Metall. Mater. Trans. A 33 (2002) 2107–2118.
[37] C.A. Siqueira, N. Cheung, A. Garcia, The columnar to equiaxed transition during solidification of Sn–Pb alloys, J. Alloys Compd. 351 (2003) 126–134.
[38] J.E. Spinelli, I.L. Ferreira, A. Garcia, Influence of melt convection on the columnar to equiaxed transition and microstructure of downward unsteady-state directionally solidified Sn–Pb alloys, J. Alloys Compd. 384 (2004) 217–226.
[39] M.V. Canté, K.S. Cruz, J.E. Spinelli, A. Garcia, Experimental analysis of the columnar-to-equiaxed transition in directionally solidified Al-Ni and Al-Sn alloys, Mater. Lett. 61 (2007) 2135–2138.
[40] S.T. Lim, I.S. Eun, S.W. Nam, Control of equilibrium phases (M,T,S) in the modified aluminum alloy 7175 for thick forging applications, Mater. Trans. 44–1 (2003) 181–187.
[41] V. Raghavan, Al-Mg-Zn (Aluminum-Magnesium-Zinc), J. Phase Equilibria Diffusion 28– 2 (2007) 203–208.
[42] O. Alvarez, C. Gonzalez, G. Aramburo, R. Herrera, J.A. Juarez-Islas, Characterization and prediction of microstructure in Al-Zn-Mg alloys, Mater. Sci. Eng. A 402 (2005) 320–324.
[43] J. Soto, G. Aramburo, C. Gonzalez, J. Genesca, R. Herrera, J.A. Juarez-Islas, Distribution and prediction of solute in Al-Zn-Mg alloys, Mater. Sci. Eng. A 408 (2005) 303–308.
[44] J. Gubicza, I. Schiller, N.Q. Chinh, J. Illy, Z. Horita, T.G. Langdon, The effect of severe plastic deformation on precipitation in supersaturated Al-Zn-Mg alloys, Mater. Sci. Eng. A 460–461 (2007) 77–85.
[45] A.L. Ramirez-Ledesma, R.A. Rodríguez-Díaz, J. Chavez-Carvayar, O. Alvarez-Fregoso, J.A. Juarez-Islas, Effect of growth rate on microstructure and solute distribution of Al–Zn–Mg alloy, Trans. Nonferrous Met. Soc. China 25 (2015), 1391–139.
[46] J.M.V. Quaresma, C.A. Santos, A. Garcia, Correlation between unsteady-state solidification conditions, dendrite spacings and mechanical properties of Al-Cu alloys, Metall. Mater. Trans. A 31–12 (2000) 3167–3178.
[47] W.R.R. Osório, A. Garcia, Modeling dendritic structure and mechanical properties of Zn Al alloys as a function of solidification conditions, Mater. Sci. Eng. A 325 (2002) 103–111.
[48] W.R.R. Osório, C.A. Santos, J.M.V. Quaresma, A. Garcia, Mechanical properties as a function of thermal parameters and microstructure of Zn Al castings, J. Mater. Process. Technol. 143–144 (2003) 703–709.
[49] P. Goulart, J.E. Spinelli, W.R.R. Osório, A. Garcia, Mechanical properties as a function of microstructure and solidification thermal variables of Al Si castings, Mater. Sci. Eng. A 421 (2006) 245–253.
[50] G. Santos, C. De Moura Neto, W.R.R. Osório, A. Garcia, Design of mechanical properties of a Zn27Al alloy based on microstructure dendritic array spacing, Mater. Des. 28 (2007) 2425–2430.
[51] W.R.R. Osório, J.E. Spinelli, C.R.M. Afonso, L.C. Peixoto, A. Garcia, Microstructure, corrosion behaviour and microhardness of a directionally solidified Sn-Cu solder alloy, Electrochim. Acta 56 (2011) 8891–8899.
[52] M.V. Canté, J.E. Spinelli, N. Cheung, A. Garcia, The correlation between dendritic microstructure and mechanical properties of directionally solidified hypoeutectic Al-Ni alloys, Met. Mater. Int. 16 (2010) 39–49.
[53] B. Silva, I. Araujo, W. Silva, P. Goulart, A. Garcia, J.E. Spinelli, Correlation between dendrite arm spacing and microhardness during unsteady-state directional solidification of Al-Ni alloys, Phil. Mag. Lett. 91 (2011) 337–343.
[54] W.R.R. Osório, D.R. Leiva, L.C. Peixoto, L.R. Garcia, A. Garcia, Mechanical properties of Sn-Ag lead-free solder alloys based on the dendritic array and Ag3Sn morphology, J. Alloys Compd. 562 (2013) 194–204.
[55] J.E. Spinelli, A. Garcia, Microstructural development and mechanical properties of hypereutectic Sn Cu solder alloys, Mater. Sci. Eng. A 568 (2013) 195–201.
[56] B.R. Porás, R.P. França, J.A. Spim, A. Garcia, E.M. Costa, C.A. Santos, The effects of dendrite arm spacings (as-cast) and aging time (solution heat-treated) of Al-Cu alloy on hardness, J. Alloys Compd. 549 (2013) 324–335.
[57] E. Acer, E. Çadırlı, H. Erol, T. Kırındı, M. Gündüz, Effect of heat treatment on the microstructures and mechanical properties of Al-5.5Zn-2.5Mg alloy, Mater. Sci. Eng. A 26 (2016) 144–156.
[58] A.D. Isadare, B. Aremo, M.O. Adeoye, O.J. Olawale, M.D. Shittu, Effect of heat treatment on some mechanical properties of 7075 aluminium alloy, J. Mater. Res. 16–1 (2013) 190–194.
[59] D.P. Mondal, S. Das, R.N. Rao, M. Singh, Effect of SiC addition and running-in-wear on the sliding wear behavior of Al-Zn-Mg aluminium alloy, Mater. Sci. Eng. A 402 (2005) 307–319.
[60] M.S. Prabhudev, V. Auradi, K. Yenkateswarlu, N.H. Siddalingswamy, S.A. Kori, Influence of Cu addition on dry sliding wear behavior of A356 alloy, Proced. Eng. 97 (2014) 1361–1367.